A three–dimensional study of the onset of convection in a horizontal, rectangular porous channel heated from below

A. Barletta[a,*]; **L. Storesletten**[b]

[a] *DIENCA, Alma Mater Studiorum – Università di Bologna,*

Viale Risorgimento 2, I–40136 Bologna, Italy

antonio.barletta@unibo.it

[b] *Department of Mathematics, University of Agder,*

Postboks 422, 4604 Kristiansand, Norway

leiv.storesletten@uia.no

Abstract The onset of convection is studied in a rectangular channel filled with a fluid saturated porous medium, bounded above and below by impermeable isothermal walls at unequal temperatures and laterally by partially conducting walls. A three–dimensional linear stability analysis is carried out under the assumption of an infinite longitudinal channel length. Then, this assumption is relaxed in order to determine the threshold length for the three–dimensional convection to be the preferred mode at onset. Sensible parameters influencing the conditions for the instability are the aspect ratio of the transverse cross–section and the Biot number associated with the sidewall heat transfer to the external environment. The neutral stability is investigated by expressing the Darcy–Rayleigh number as a function of the longitudinal wave number, for assigned values of the transverse aspect ratio and of the Biot number.

Keywords Rectangular channel; Darcy–Bénard problem; Linear stability; Method of weighted residuals; Biot number; Lateral confinement.

*Corresponding author

Nomenclature

a	dimensionless wave number, Eq. (13)
A, A_m, C_m	dimensionless coefficients, Eqs. (16) and (20)
B	Biot number, Eq. (5)
c	heat capacity per unit mass
d	dimensionless channel length, D/H
D	channel length
$\mathbf{e}_y$	unit vector in the y–direction
E_P, E_θ	dimensionless residuals, Eq. (23)
$\mathbf{g}$; g	gravitational acceleration; modulus of $\mathbf{g}$
h	external heat transfer coefficient, Eq. (2)
H	channel height
i, j, n, N, m	natural numbers
k	thermal conductivity
K	permeability
L	channel half–thickness
m_0	natural number, Eq. (42)
$\underset{\sim}{M}$	dimensionless matrix, Eqs. (27)–(30)
p	dimensionless pressure, Eq. (3)
p_0	dimensionless reference pressure, Eq. (7)
P	dimensionless pressure disturbance, Eq. (10)
$\widetilde{P}, \widetilde{\theta}$	dimensionless disturbance amplitudes, Eq. (13)
R	Darcy–Rayleigh number, Eq. (5)
s	aspect ratio, Eq. (5)
t	dimensionless time, Eq. (3)
T	dimensionless temperature, Eq. (3)
T_0	temperature of the upper boundary $\overline{y} = H$, Eq. (2)
$\mathbf{u}$	dimensionless velocity, (u, v, w), Eq. (3)
$\mathbf{x}$	dimensionless position vector, (x, y, z), Eq. (3)
$\underset{\sim}{X}$	dimensionless vector of the coefficients, Eq. (25)

Greek symbols

α	thermal diffusivity, $k/(\rho c)$

β	thermal expansion coefficient
ΔT	constant temperature difference, Eq. (2)
ε	dimensionless perturbation parameter, Eq. (10)
ζ_1, ζ_2	dimensionless parameters, Eq. (39)
η	dimensionless parameter, Eq. (38)
θ	dimensionless temperature disturbance, Eq. (10)
λ_m	dimensionless roots of Eq. (22)
μ	dynamic viscosity
ρ	density
φ_m, ψ_m	dimensionless test functions, Eq. (20)
σ	heat capacity ratio of the porous medium
ω	dimensionless parameter, Eq. (19)
Ω_1, Ω_2	dimensionless parameters, Eq. (39)

Superscript, subscripts

$\bar{}$	dimensional quantity
b	basic solution
c	critical value
th	threshold value
$'$	differentiation with respect to x
$\lceil \cdot \rceil$	ceiling function

1 Introduction

The study of the conditions for the onset of convection in a fluid saturated porous medium heated from below gave rise to a wide literature through the last six decades. The large amount of papers published on this subject were originated by the pioneering studies of Horton and Rogers [1], and Lapwood [2]. Reviews of this topic, classified either as Darcy–Bénard problem or as Horton–Rogers–Lapwood problem, are available in Rees [3], Tyvand [4], Nield and Bejan [5], Straughan [6], Barletta [7]. The interest on thermal convection in a porous medium due to an underlying heat source are strictly related, for instance, to the groundwater flow in geothermal sites, as well as to the diffusion of pollutants or of nuclear waste in the soil. The original statement of the Darcy–Bénard problem is relative

to an infinitely wide horizontal porous layer saturated by a fluid at rest in the basic state, such that the momentum balance is modelled by Darcy's law, bounded by two horizontal walls, plane, impermeable, perfectly conducting and with unequal uniform temperatures. Several investigators explored diverse variants of the elementary Darcy–Bénard problem including, among the many possible effects originally neglected, the presence of a horizontal or vertical throughflow, the inclination of the layer to the horizontal, the non–Darcian nature of the momentum transfer, the lateral confinement of the porous medium due to sidewalls. The issue of lateral confinement is closely related to the more general issue of the role played by the shape of the transverse cross–section of the porous medium in comparison with the plane–parallel geometry considered in the original Darcy–Bénard problem. Hence, a rectangular cross–section means lateral confinement with vertical plane sidewalls. We point out that lateral confinement implies that the porous medium is in fact a porous channel with infinite or finite length along the longitudinal direction. The case of a horizontal porous channel with circular cross–section was studied by Storesletten and Tveitereid [8] and, more recently, by Barletta and Storesletten [9]. The onset of two–dimensional convection in the case of a porous channel with a general cross–section was studied by Rees and Tyvand [10]. These authors formulated the linear stability analysis in terms of the eigenmodes of the Helmholtz equation in an arbitrary two–dimensional domain. We mention that the instability is not necessarily two–dimensional, but it may be three–dimensional provided that the longitudinal length of the channel is sufficiently large [8, 9].

The investigation of the Darcy–Bénard problem in a rectangular channel was initiated by Sutton [11], Beck [12] and further developed by Nilsen and Storesletten [13]. An interesting survey on this topic can be found in Holzbecher [14]. Beck [12] carried out the analysis of the Darcy–Bénard problem in a three–dimensional porous box, *i.e.* a rectangular channel with a finite longitudinal length, laterally bounded by impermeable and adiabatic walls. The analytical solution carried out by this author evidences that the critical value of the Darcy–Rayleigh number for the onset of the instability may be, depending on the aspect ratios of the box, greater or equal to $4\pi^2$, namely the critical value found in the limit of a porous layer with an infinite horizontal width. Nilsen and Storesletten [13] studied the two–dimensional stability of a fluid saturated porous medium, either isotropic or anisotropic, in a short rectangular channel laterally bounded by perfectly conducting impermeable walls. These authors were able to determine the critical conditions for the

linear stability of the two–dimensional modes showing, in agreement with Beck [12], that the lateral confinement produces an enhanced stability of the porous medium. Obviously, the interest of their results relies in the analysis of a different kind of lateral confinement with respect to Beck [12]: perfectly conducting sidewalls instead of adiabatic sidewalls. Rees and Tyvand [15] explored a case where the vertical sidewalls of the two–dimensional porous cavity have asymmetric boundary conditions: one impermeable and perfectly conducting, the other open and thermally insulating. Interestingly enough, Rees and Tyvand [15] showed that the asymmetry in the lateral confinement conditions implies that the onset of the linear instability is through oscillatory modes. Further results relative to the onset of oscillatory convection can be found in Holzbecher [14, 16]. Recently, Nygård and Tyvand [17] proposed an extension of the analysis by Nilsen and Storesletten [13] on modelling the sidewalls as partially permeable and partially conducting.

A common feature of the papers by Nilsen and Storesletten [13], Rees and Tyvand [15] and Nygård and Tyvand [17] is that they are based on a two–dimensional analysis, while three–dimensional modes may be dominant at the onset of convection, as proved by Beck [12], as well as by Storesletten and Tveitereid [8] in the case of a horizontal circular channel. The purpose of our study is to extend the analysis drawn by Nilsen and Storesletten [13] along two directions: we assume partially conducting lateral walls; we carry out a three–dimensional linear stability analysis for a channel with a longitudinal infinite length. At the end of our analysis, we will also explore the effect of a finite longitudinal length. The linear disturbance equations are solved by Galerkin's method of weighted residuals, as well as by a sixth–order Runge–Kutta method combined with the shooting method. The thermal behaviour of the vertical sidewalls is modelled through a Biot number associated with the convection to an external, thermally stratified, fluid environment. The limit of a zero Biot number and that of an infinite Biot number correspond to the special cases investigated by Beck [12] and by Nilsen and Storesletten [13], respectively.

2 Mathematical model

We consider natural convection in a horizontal rectangular channel filled with a fluid saturated porous medium and heated from below. The channel is rectangular with height H, width $2L$, and with an infinite length. We choose a Cartesian coordinate system with the $\overline{y}$–axis in the vertical direction and the $\overline{x}$–axis in the horizontal direction perpendicular

to the channel axis. The horizontal channel walls are at $\overline{y} = 0$ and $\overline{y} = H$, and the vertical walls at $\overline{x} = -L$ and $\overline{x} = L$; see Fig. 1. Relative to the Cartesian set of coordinates $(\overline{x}, \overline{y}, \overline{z})$, the components of the seepage velocity $\overline{\mathbf{u}}$ are denoted as $(\overline{u}, \overline{v}, \overline{w})$, respectively. We assume that the effect of viscous dissipation is negligible and that the solid and fluid phases are in local thermal equilibrium. Then, the local balance equations for mass, momentum and energy can be written as

$$\overline{\boldsymbol{\nabla}} \cdot \overline{\mathbf{u}} = 0, \tag{1a}$$

$$\frac{\mu}{K}\overline{\mathbf{u}} = -\overline{\boldsymbol{\nabla}}\overline{p} + \rho g \beta \left(\overline{T} - T_0\right) \mathbf{e}_y, \tag{1b}$$

$$\sigma \frac{\partial T}{\partial t} + \overline{\mathbf{u}} \cdot \overline{\boldsymbol{\nabla}}\, \overline{T} = \alpha \overline{\nabla}^2 \overline{T}. \tag{1c}$$

where $\mathbf{e}_y$ is the unit vector along the vertical $\overline{y}$–axis, and σ is the ratio between the average volumetric heat capacity of the fluid saturated porous medium and the volumetric heat capacity of the fluid.

The channel walls are assumed to be impermeable. We assume that the upper and lower horizontal walls are isothermal at temperatures T_0 and $T_0 + \Delta T$, respectively. The lateral walls are partially conducting and exchange heat with an external fluid environment, thermally stratified in the vertical direction, so that the boundary conditions are:

$$\begin{aligned}
&\overline{v} = 0, \quad \overline{T} = T_0 + \Delta T, \quad \text{on } \overline{y} = 0,\ -L < \overline{x} < L, \\
&\overline{v} = 0, \quad \overline{T} = T_0, \quad \text{on } \overline{y} = H,\ -L < \overline{x} < L, \\
&\overline{u} = 0, \quad -k\frac{\partial \overline{T}}{\partial \overline{x}} = \pm h \left[\overline{T} - T_0 - \Delta T \left(1 - \frac{\overline{y}}{H}\right)\right], \quad \text{on } \overline{x} = \pm L,\ 0 < \overline{y} < H.
\end{aligned} \tag{2}$$

The same temperature conditions at the lateral boundary were adopted by Barletta and Storesletten [9] with reference to a circular duct. Moreover, a similar thermal model of the sidewalls was formulated by Nygård and Tyvand [17] and Nygård and Tyvand [18]. We mention that these authors relaxed also the impermeability conditions for the velocity by assuming partially penetrative sidewalls.

2.1 Dimensionless equations

The dimensional fields, coordinates, time and nabla operator are denoted by an overline. The corresponding dimensionless quantities are defined such that

$$\begin{aligned}
&(\overline{x}, \overline{y}, \overline{z}) = (x, y, z)\ H, \quad (\overline{u}, \overline{v}, \overline{w}) = (u, v, w)\ \frac{\alpha}{H}, \quad \overline{\boldsymbol{\nabla}} = \frac{1}{H}\ \boldsymbol{\nabla}, \\
&\overline{T} = T_0 + T\ \Delta T, \quad \overline{p} = p\ \frac{\mu\alpha}{K}, \quad \overline{t} = t\ \frac{\sigma H^2}{\alpha}.
\end{aligned} \tag{3}$$

The governing equations (1) and (2) can be rewritten in a dimensionless form as

$$\boldsymbol{\nabla} \cdot \mathbf{u} = 0, \tag{4a}$$

$$\mathbf{u} = -\boldsymbol{\nabla} p + RT\mathbf{e}_y, \tag{4b}$$

$$\frac{\partial T}{\partial t} + \mathbf{u} \cdot \boldsymbol{\nabla} T = \nabla^2 T. \tag{4c}$$

The Darcy–Rayleigh number R, the Biot number B, and the aspect ratio s are given by

$$R = \frac{\rho g \beta K H \Delta T}{\mu \alpha}, \quad B = \frac{hH}{k}, \quad s = \frac{L}{H}. \tag{5}$$

For the definition and the physical meaning of the Biot number see, for instance, page 284 of Incropera et al. [19].

The boundary conditions Eq. (2) can be rewritten as

$$\begin{aligned} &v = 0, \quad T = 1, \quad \text{on } y = 0,\ -s < x < s, \\ &v = 0, \quad T = 0, \quad \text{on } y = 1,\ -s < x < s, \\ &u = 0, \quad \frac{\partial T}{\partial x} \pm B\,(T - 1 + y) = 0, \quad \text{on } x = \pm s,\ 0 < y < 1. \end{aligned} \tag{6}$$

The limiting cases $B \to \infty$ and $B \to 0$ correspond to perfectly conducting sidewalls and perfectly insulating (adiabatic) sidewalls, respectively.

2.2 Basic solution

A stationary solution of Eqs. (4) and (6) is given by

$$u_b = v_b = w_b = 0, \quad T_b = 1 - y, \quad p_b = p_0 + Ry\left(1 - \frac{y}{2}\right), \tag{7}$$

where "b" stands for "basic solution", and p_0 is an arbitrary integration constant.

3 Linear disturbances

Let us first eliminate the velocity components (u, v, w) by substituting Eq. (4b) into Eqs. (4a) and (4c), which yields

$$\nabla^2 p = R\frac{\partial T}{\partial y}, \tag{8a}$$

$$\frac{\partial T}{\partial t} - \boldsymbol{\nabla} p \cdot \boldsymbol{\nabla} T + RT\frac{\partial T}{\partial y} = \nabla^2 T. \tag{8b}$$

The boundary conditions now become

$$\begin{aligned}
&\frac{\partial p}{\partial y} = R, \quad T = 1, \quad \text{on } y = 0,\ -s < x < s, \\
&\frac{\partial p}{\partial y} = 0, \quad T = 0, \quad \text{on } y = 1,\ -s < x < s, \\
&\frac{\partial p}{\partial x} = 0, \quad \frac{\partial T}{\partial x} \pm B\,(T - 1 + y) = 0, \quad \text{on } x = \pm s,\ 0 < y < 1.
\end{aligned} \tag{9}$$

We perturb the basic solution, Eq. (7), with small amplitude disturbances defined by

$$p = p_b + \varepsilon P, \quad T = T_b + \varepsilon\theta. \tag{10}$$

Following the usual linear stability analysis, we substitute Eq. (10) into Eqs. (8) neglecting the terms of order ε^2. Thus, we obtain

$$\nabla^2 P = R\frac{\partial \theta}{\partial y}, \tag{11a}$$

$$\nabla^2 \theta = \frac{\partial \theta}{\partial t} - R\theta + \frac{\partial P}{\partial y}, \tag{11b}$$

subject to the boundary conditions

$$\begin{aligned}
&\frac{\partial P}{\partial y} = 0, \quad \theta = 0, \quad \text{on } y = 0,\ -s < x < s, \\
&\frac{\partial P}{\partial y} = 0, \quad \theta = 0, \quad \text{on } y = 1,\ -s < x < s, \\
&\frac{\partial P}{\partial x} = 0, \quad \frac{\partial \theta}{\partial x} \pm B\theta = 0, \quad \text{on } x = \pm s,\ 0 < y < 1.
\end{aligned} \tag{12}$$

4 Normal modes

For the analysis of the neutral stability, we are interested in the time–independent solutions of Eqs. (11) and (12). Following the usual normal mode decomposition, we may write

$$\begin{aligned}
&P(x, y, z) = \widetilde{P}(x)\cos(n\pi y)\cos(az), \\
&\theta(x, y, z) = \widetilde{\theta}(x)\sin(n\pi y)\cos(az), \qquad n = 1, 2, 3, \ \ldots\ .
\end{aligned} \tag{13}$$

where a is the dimensionless wave number. We note that $a = 0$ means two–dimensional modes of convective instability.

We substitute Eq. (13) into Eqs. (11) and (12), so that we obtain

$$\widetilde{P}'' - \left(a^2 + n^2\pi^2\right)\widetilde{P} - Rn\pi\widetilde{\theta} = 0, \tag{14a}$$

$$\widetilde{\theta}'' - \left(a^2 + n^2\pi^2 - R\right)\widetilde{\theta} + n\pi\widetilde{P} = 0, \tag{14b}$$

with the boundary conditions

$$\widetilde{P}' = 0, \quad \widetilde{\theta}' \pm B\widetilde{\theta} = 0, \quad \text{on } x = \pm s, \tag{15}$$

where primes denote differentiation with respect to x.

4.1 The special case $B \to 0$

In this limiting case, originally studied by Beck [12], the solution of Eqs. (14) and (15) is given by

$$\begin{aligned} \widetilde{P}(x) &= A\cos\left[\frac{(m-1)\pi}{2s}(x+s)\right], \\ \widetilde{\theta}(x) &= \cos\left[\frac{(m-1)\pi}{2s}(x+s)\right], \qquad m = 1, 2, 3 \ \ldots \ . \end{aligned} \tag{16}$$

where A is a constant that can be determined, together with the eigenvalue R, on substituting Eq. (16) into Eqs. (14), namely

$$A = -\frac{Rn\pi}{a^2 + \dfrac{(m-1)^2\pi^2}{4s^2} + n^2\pi^2}, \quad R = \frac{\left[a^2 + \dfrac{(m-1)^2\pi^2}{4s^2} + n^2\pi^2\right]^2}{a^2 + \dfrac{(m-1)^2\pi^2}{4s^2}}, \tag{17}$$

with $m = 1, 2, 3 \ \ldots$, and $n = 1, 2, 3 \ \ldots$.

We can conclude that, for every pair (m, s), the lowest neutral stability curve $R(a)$ is for $n = 1$. As a consequence, the critical conditions for the onset of the instability (a_c, R_c) are determined by setting $n = 1$ in Eq. (17) and imposing that the derivative $\partial R/\partial a$ be zero for a given pair (m, s). By this method, we obtain

$$a_c = \pi\left[1 - \frac{(m-1)^2}{4s^2}\right]^{1/2}, \quad R_c = 4\pi^2. \tag{18}$$

The critical condition defined by Eq. (18) is accomplished with any $m = 1, 2, 3 \ \ldots$ such that $m \leq 2s + 1$. The inequality $m \leq 2s + 1$ can be satisfied just by the mode $m = 1$ and also by higher m–modes, depending on how large is the aspect ratio s. In other words, at the onset of the instability, we may have more than one critical wave number a_c corresponding to $R_c = 4\pi^2$. For every $s < 1/2$, *i.e.* for every tall rectangular cross–section, only the mode $m = 1$ yields $R_c = 4\pi^2$. For instance, in the case of a channel with a square cross–section ($s = 1/2$), we obtain the critical Darcy–Rayleigh number $R_c = 4\pi^2$ either with $a_c = \pi$ (mode $m = 1$) or with $a_c = 0$ (mode $m = 2$). From Eq. (16), we immediately conclude that the eigenfunctions $\widetilde{P}(x)$ and $\widetilde{\theta}(x)$ are odd functions when m is even, and are even functions when m is odd.

Figure 2 displays the neutral stability curves $R(a)$ with four different aspect ratios, $s = 3/2, 1, 1/2, 1/4$. These aspect ratios were selected to illustrate the changes on shifting from shallow to tall rectangular cross–sections. We selected different plotting regions for the different aspect ratios, since on decreasing the aspect ratio s the neutral stability

curves tend to move upwards in the (a, R)–plane. For each frame, we drew all the curves contained in the chosen plotting region. The frames with $s = 3/2, 1, 1/2$ contain only curves for the modes with $n = 1$ and different values of m. The frame corresponding to the tall rectangle, $s = 1/4$, contains within the plotting region also two neutral stability curves with $n = 2$. In particular, the curves whose minimum is $R = 4\pi^2$ are determined through the inequality $m \leq 2s + 1$. Hence, we have four curves with $s = 3/2$ ($n = 1$ and $m = 1, 2, 3, 4$), three curves with $s = 1$ ($n = 1$ and $m = 1, 2, 3$), two curves with $s = 1/2$ ($n = 1$ and $m = 1, 2$), and just one curve with $s = 1/4$ ($n = 1$ and $m = 1$).

5 A Galerkin weighted residuals solution

In the general case, $B > 0$, the m–modes are not independent with each other as in the limit $B \to 0$. For convenience, we introduce the parameter

$$\omega = 2Bs. \tag{19}$$

Hence, we express the solution of Eqs. (14) and (15) as

$$\widetilde{P}(x) = \sum_{m=1}^{\infty} A_m \varphi_m(x), \qquad \widetilde{\theta}(x) = \sum_{m=1}^{\infty} C_m \psi_m(x), \tag{20}$$

where the test functions $\varphi_m(x)$ and $\psi_m(x)$ are chosen so that Eq. (15) is satisfied, namely

$$\begin{aligned} \varphi_m(x) &= \cos\left[\frac{(m-1)\pi}{2s}(x+s)\right], \\ \psi_m(x) &= \cos\left[\frac{\lambda_m}{2s}(x+s)\right] + \frac{\omega}{\lambda_m}\sin\left[\frac{\lambda_m}{2s}(x+s)\right], \qquad m = 1, 2, 3 \ \ldots \ . \end{aligned} \tag{21}$$

The coefficients λ_m are, for every $\omega > 0$, the positive roots of

$$\left(\omega^2 - \lambda_m^2\right)\tan\lambda_m + 2\omega\lambda_m = 0. \tag{22}$$

In the special case $B \to 0$ (or $\omega \to 0$), one has $\lambda_m = (m-1)\pi$, so that exactly the same m–modes obtained in section 4.1 are recovered.

On substituting Eqs. (20) and (21) into Eqs. (14), we obtain the residuals

$$E_P(x) = \sum_{m=1}^{\infty}\left\{A_m\left[a^2 + \frac{(m-1)^2\pi^2}{4s^2} + n^2\pi^2\right]\varphi_m(x) + C_m R n\pi\psi_m(x)\right\}, \tag{23a}$$

$$E_\theta(x) = \sum_{m=1}^{\infty}\left[A_m n\pi\varphi_m(x) - C_m\left(a^2 + \frac{\lambda_m^2}{4s^2} + n^2\pi^2 - R\right)\psi_m(x)\right]. \tag{23b}$$

Following the procedure described in Finlayson and Scriven [20] and in Finlayson [21], we prescribe the orthogonality of $E_P(x)$ with respect to the test functions $\varphi_i(x)$, and the orthogonality of $E_\theta(x)$ with respect to the test functions $\psi_i(x)$,

$$\int_{-s}^{s} E_P(x)\varphi_i(x)\mathrm{d}x = 0, \quad \int_{-s}^{s} E_\theta(x)\psi_i(x)\mathrm{d}x = 0, \qquad i = 1, 2, 3 \ \ldots \ . \tag{24}$$

We can obtain an approximate solution by considering the first N terms in the infinite sums Eqs. (23). The higher is the order N the better is the accuracy of the solution. It is convenient to define a $2N$–dimensional vector of the coefficients,

$$\underset{\sim}{X} = (A_1, A_2, \ \ldots \ , A_N, C_1, C_2, \ \ldots \ , C_N) \, . \tag{25}$$

Thus, Eq. (24) can be rewritten in a matrix form,

$$\underset{\sim}{M} \cdot \underset{\sim}{X} = 0, \tag{26}$$

where the $2N \times 2N$ matrix $\underset{\sim}{M}$ is defined by four $N \times N$ blocks, namely

$$\begin{aligned} M_{ij} &= \left[a^2 + \frac{(j-1)^2\pi^2}{4s^2} + n^2\pi^2\right] \int_{-s}^{s} \varphi_i(x)\varphi_j(x)\mathrm{d}x \\ &= \left[a^2 + \frac{(i-1)^2\pi^2}{4s^2} + n^2\pi^2\right] s\,(1+\delta_{i1}) \ \delta_{ij}, \\ &\qquad i = 1, 2, \ \ldots \ , N; \ j = 1, 2, \ \ldots \ , N, \end{aligned} \tag{27}$$

$$\begin{aligned} M_{ij} &= n\pi \int_{-s}^{s} \psi_{i-N}(x)\varphi_j(x)\mathrm{d}x \\ &= -2s\, n\pi \ \frac{\omega + (-1)^j \left(\omega \cos\lambda_{i-N} - \lambda_{i-N} \sin\lambda_{i-N}\right)}{(j-1)^2\pi^2 - \lambda_{i-N}^2}, \\ &\qquad i = N+1, N+2, \ \ldots \ , 2N; \ j = 1, 2, \ \ldots \ , N, \end{aligned} \tag{28}$$

$$\begin{aligned} M_{ij} &= Rn\pi \int_{-s}^{s} \varphi_i(x)\psi_{j-N}(x)\mathrm{d}x \\ &= -2Rs\, n\pi \ \frac{\omega + (-1)^i \left(\omega \cos\lambda_{j-N} - \lambda_{j-N} \sin\lambda_{j-N}\right)}{(i-1)^2\pi^2 - \lambda_{j-N}^2}, \\ &\qquad i = 1, 2, \ \ldots \ , N; \ j = N+1, N+2, \ \ldots \ , 2N, \end{aligned} \tag{29}$$

$$\begin{aligned} M_{ij} &= -\left(a^2 + \frac{\lambda_{j-N}^2}{4s^2} + n^2\pi^2 - R\right) \int_{-s}^{s} \psi_{i-N}(x)\psi_{j-N}(x)\mathrm{d}x \\ &= -\frac{s}{\lambda_{i-N}^2}\left(a^2 + \frac{\lambda_{i-N}^2}{4s^2} + n^2\pi^2 - R\right) \\ &\quad \times \left[\lambda_{i-N}^2 + \omega + \omega^2 + \frac{\omega\left(\lambda_{i-N}^2 + \omega^2\right)^2 \cos^2\lambda_{i-N}}{\left(\lambda_{i-N}^2 - \omega^2\right)^2}\right] \delta_{ij}, \\ &\qquad i = N+1, N+2, \ \ldots \ , 2N; \ j = N+1, N+2, \ \ldots \ , 2N. \end{aligned} \tag{30}$$

On account of Eq. (26), a nonvanishing coefficient vector $\underset{\sim}{X}$ may exist if and only if the matrix $\underset{\sim}{M}$ has a vanishing determinant,

$$\det(\underset{\sim}{M}) = 0. \tag{31}$$

The solution of Eq. (31) yields the neutral stability function $R(a)$, for every assignment of the input parameters (s, ω, n).

5.1 The limiting case $B \to \infty$

When the Biot number becomes infinitely large, the boundary conditions on $\widetilde{\theta}(x)$ become of Dirichlet type, and we have $\omega \to \infty$. Hence, a different choice of the test functions $\psi_m(x)$ is necessary, *i.e.*, Eq. (21) should be replaced by

$$\begin{aligned} \varphi_m(x) &= \cos\left[\frac{(m-1)\pi}{2s}(x+s)\right], \\ \psi_m(x) &= \sin\left[\frac{m\pi}{2s}(x+s)\right], \qquad m = 1, 2, 3 \ \ldots \ . \end{aligned} \tag{32}$$

This implies that also the elements of the matrix $\underset{\sim}{M}$ change. We have in this case

$$\begin{aligned} M_{ij} &= \left[a^2 + \frac{(j-1)^2\pi^2}{4s^2} + n^2\pi^2\right] \int_{-s}^{s} \varphi_i(x)\varphi_j(x)\mathrm{d}x \\ &= \left[a^2 + \frac{(i-1)^2\pi^2}{4s^2} + n^2\pi^2\right] s\,(1+\delta_{i1})\ \delta_{ij}, \\ &\qquad\qquad i = 1, 2, \ \ldots \ , N; \ j = 1, 2, \ \ldots \ , N, \end{aligned} \tag{33}$$

$$\begin{aligned} M_{ij} &= n\pi \int_{-s}^{s} \psi_{i-N}(x)\varphi_j(x)\mathrm{d}x \\ &= \begin{cases} \dfrac{2sn\left[1+(-1)^{i+j+N}\right](i-N)}{(i-N)^2-(j-1)^2}, & i-N \neq j-1, \\ 0, & i-N = j-1, \end{cases} \\ &\qquad i = N+1, N+2, \ \ldots \ , 2N; \ j = 1, 2, \ \ldots \ , N, \end{aligned} \tag{34}$$

$$\begin{aligned} M_{ij} &= Rn\pi \int_{-s}^{s} \varphi_i(x)\psi_{j-N}(x)\mathrm{d}x \\ &= \begin{cases} \dfrac{2Rsn\left[1+(-1)^{i+j+N}\right](j-N)}{(j-N)^2-(i-1)^2}, & i-1 \neq j-N, \\ 0, & i-1 = j-N, \end{cases} \\ &\qquad i = 1, 2, \ \ldots \ , N; \ j = N+1, N+2, \ \ldots \ , 2N, \end{aligned} \tag{35}$$

$$M_{ij} = -\left[a^2 + \frac{(j-N)^2\pi^2}{4s^2} + n^2\pi^2 - R\right]\int_{-s}^{s} \psi_{i-N}(x)\psi_{j-N}(x)\mathrm{d}x$$
$$= -s\left[a^2 + \frac{(i-N)^2\pi^2}{4s^2} + n^2\pi^2 - R\right]\delta_{ij}, \tag{36}$$
$$i = N+1, N+2, \ \ldots\ , 2N;\ j = N+1, N+2, \ \ldots\ , 2N.$$

We mention that an analytical solution for this limiting case was found by Nilsen and Storesletten [13] by restricting their analysis to the two–dimensional linear disturbances depending only on (x, y). In other words, these authors assumed $a = 0$ (short channels) and found, for the lowest mode of neutral stability,

$$R(0) = 4\pi^2\left(1 + \frac{1}{4s^2}\right). \tag{37}$$

6 Numerical solution

The solution based on the Galerkin method of weighted residuals, described in Section 5, provides a fast and reliable procedure for a graphical representation of the neutral stability curves $R(a)$. A slower, but more accurate, solution procedure is a sixth–order Runge–Kutta method. This procedure is for solving Eqs. (14) as an initial value problem starting from $x = -s$. The initial conditions coming from Eq. (15) have to be completed with

$$\widetilde{P}(-s) = \eta, \quad \widetilde{\theta}(-s) = 1. \tag{38}$$

The first of these conditions defines an unknown parameter η to be determined, together with the eigenvalue $R(a)$, through a shooting method that ensures the fulfillment of the target conditions at $x = s$, Eq. (15). The second equation (38) fixes the overall scale of the solution $(\widetilde{P}, \widetilde{\theta})$, otherwise indeterminate due to the homogeneity of Eqs. (14) and (15). The combined Runge–Kutta method and shooting method are implemented within the software Mathematica 8 (© Wolfram, Inc.) by means of the built–in functions `NDSolve` and `FindRoot`, respectively. In the following, the graphics of the neutral stability curves $R(a)$ are obtained by the Galerkin method of weighted residuals, described in Section 5, whereas the numerical method described in this section is used to check the graphics of $R(a)$ and to obtain accurate values for the specially interesting points, such as the local minima.

We mention that Eqs. (14) and (15) could have been solved by expressing both $\widetilde{P}(x)$ and $\widetilde{\theta}(x)$ as linear combinations of the modes

$$\cos(\Omega_1\, x + \zeta_1)\,, \quad \cos(\Omega_2\, x + \zeta_2)\,, \tag{39}$$

where Ω_1 and Ω_2 are given by

$$\begin{aligned}\Omega_1 &= \sqrt{\frac{1}{2}\left[R - 2\,(a^2 + n^2\pi^2) - \sqrt{R(R - 4\,n^2\pi^2)}\right]}\,,\\ \Omega_2 &= \sqrt{\frac{1}{2}\left[R - 2\,(a^2 + n^2\pi^2) + \sqrt{R(R - 4\,n^2\pi^2)}\right]}\,.\end{aligned} \tag{40}$$

The phase coefficients ζ_1 and ζ_2 have to be determined numerically, together with the eigenvalue R, by solving the set of algebraic equations obtained from the boundary conditions, Eq. (15), for prescribed values of (a, s, B, n). This elegant solution, brought to our attention by one of the anonymous reviewers, is a valid alternative to the numerical solution based on sixth–order Runge–Kutta method and on the shooting method.

7 Discussion of the results

In Section 5, we pointed out that the neutral stability curves $R(a)$ are determined by the equation $\det(\underset{\sim}{M}) = 0$. The limiting case $B \to 0$ is special, as the matrix $\underset{\sim}{M}$ is diagonal in this case. This conclusion is easily inferred from Sections 4 and 5. Thus, the m–modes are independent when $B \to 0$, whereas they become entangled for $B > 0$. When $B \to 0$, we have different branches of neutral stability each one identified by a value of m, as it is shown in Fig. 2. The mixing up of the m–modes implies that this identification is ruled out when $B > 0$.

7.1 A shallow rectangular channel, $s = 1$

Figures 3 and 4 are for the aspect ratio $s = 1$ and show the effect of increasing the Biot number on the shape of the neutral stability curves. When $B = 1/10$, we have a shape quite similar to that displayed in the top right frame of Fig. 2. We see that the effect of a small Biot number is to pinch off the intersection point of the $m = 1$ and $m = 3$ branches, and likewise for the $m = 2$ and $m = 4$ branches. This is a typical effect of the modes entanglement at $B > 0$: we have a mixing up of the modes with an odd m, as well as of the modes with an even m. With $B = 1/2$, we notice that the disconnected upper and lower parts of the mixed $(m = 1, m = 3)$–branch are more distant, while the upper part of the $(m = 2, m = 4)$–branch disappeared being moved upward of the plotting area. A continuous deformation of the neutral stability curves is perceived as B further increases with a progressive separation of the different branches. From $B = 5$ (Fig. 3) to $B = 10$ (Fig. 4), we see that the two branches move upward and become closer. In

the limit $B \to \infty$, the two branches eventually touch at $a = 0$ (with $R = 49.3480$) and intersect at $a = 1.273$ (with $R = 47.65$). Indeed, $R(0) = 49.34802$ perfectly agrees with the prediction of Eq. (37), $R(0) = 5\pi^2$, coming from the analytical solution found by Nilsen and Storesletten [13] for short channels. Moreover, with $B \to \infty$, the eigenvalue $R(0)$ appears to be degenerate as it results simultaneously from the two branches of neutral stability. This circumstance is in agreement with the findings of Nilsen and Storesletten [13]. These authors evidenced the degeneracy of $R(0)$ for every aspect ratio. An important feature illustrated in Figs. 3 and 4, as compared to Fig. 2, is that the absolute minimum of neutral stability is never at $a = 0$, except for the limiting case $B \to 0$. As a consequence, convection is three-dimensional and not two–dimensional at its onset. This statement is true at least for a channel infinitely long in the z–direction; we will show later on that the onset of the convective instability may be through two–dimensional patterns when the length of the channel is finite and sufficiently small.

7.2 A square channel, $s = 1/2$

The gradual change of the neutral stability curves when the Biot increases above zero is illustrated in Figs. 5 and 6, with reference to a channel with a square cross–section ($s = 1/2$). The behaviour, on a qualitative ground, is quite similar to that described for a shallow rectangular channel. On comparing the neutral stability curves for $B \to 0$ (Fig. 2) with those for $B = 1/10$, we note that the intersection of the curves for the modes $m = 1$ and $m = 3$ is pinched off with $B = 1/10$ due to the mixing up of the m–modes. The two resulting branches move away from each other as B further increases, and the upper branch disappears for $B = 5$ from the plotting area. When the limit $B \to \infty$ is approached, the two remaining curves touch at $a = 0$ (with $R(0) = 78.9568$). Again, this result is in excellent agreement with Eq. (37), $R(0) = 8\pi^2$, and again the two–dimensional convection ($a = 0$) is not the most unstable pattern at onset. We mention that, unlike what we found in the case $s = 1$ with $B \to \infty$, we have now no further intersections between the neutral stability curves at $a > 0$.

7.3 A tall rectangular channel, $s = 1/4$

The case of a tall rectangular channel, $s = 1/4$, involves higher values of R than the cases $s = 1, 1/2$. Figures 7 and 8 display the modification of the neutral stability curves with an increasing Biot number. As for the other aspect ratios, a comparison with the limiting case

$B \to 0$ reveals that the neutral stability curves for $B = 1/10$ are barely different, and that the intersection of the $(n = 1, m = 1)$ and $(n = 1, m = 3)$ is pinched off when B increases above zero. The branches for the lowest $n = 2$ modes slowly move upwards as B increases with the values $1/10, 1/2, 1$ and, eventually, the branch $(n = 2, m = 2)$ disappears above the plotting region when $B = 5$. We may track the changes of the two lower branches, originated from the curves $(n = 1, m = 1)$, $(n = 1, m = 2)$ and $(n = 1, m = 3)$ of the case $B \to 0$, as B increases above 5 (Figs. 7 and 8). We see that the end points, at $a = 0$, of these branches slowly rise upwards and eventually touch in the limit $B \to \infty$, with a value $R(0) = 197.392$, in excellent agreement with the analytical expression found by Nilsen and Storesletten [13], Eq. (37), namely $R(0) = 20\pi^2$.

7.4 The critical conditions for the onset of the instability

Figure 2 illustrates the main feature of the limiting case $B \to 0$: several values of the wave number a may yield the critical value for the onset of convection $R_c = 4\pi^2$. How many depends on the aspect ratio s; the smaller is s the less are the possible wave numbers yielding $R_c = 4\pi^2$. This feature is not observed when B increases above 0. In particular, R_c is higher than $4\pi^2$ when $B > 0$, and this critical value is displayed as the local minimum of a specific branch of neutral stability: that originated from the mode $(n = 1, m = 1)$ of the limiting case $B \to 0$. In other words, if $B > 0$, the critical value of the Darcy–Rayleigh number, R_c, yields a neutral stability condition with a three–dimensional convection pattern, since $a_c > 0$. Figure 9 shows the change of R_c with B for the three different aspect ratios, $s = 1, 1/2, 1/4$, considered in Figs. 3–8. We see that the main feature, *i.e.* that R_c is a monotonic increasing function of B, is common to the three aspect ratios considered. Figure 10 shows the change of a_c with B. The critical wave number does not vary monotonically with B. For $s = 1$, we have a local maximum of a_c when $B = 0.229$. For $s = 1/2$, we have an even more marked local maximum for $B = 4.27$. In the case of the tall rectangular channel ($s = 1/4$), there is a barely visible local maximum of a_c versus B, for $B = 154$. We note that, both for $s = 1/2$ and $s = 1/4$, the asymptotic value of a_c for $B \to \infty$ is higher than the limiting value $a_c = \pi$ for $B \to 0$. The reverse holds for the shallow rectangular channel.

In Tables 1–3, the critical values (a_c, R_c) for the onset of convection are reported versus B, together with the corresponding values of $R(0)$. With $R(0)$ we denote the lowest eigenvalue R corresponding to $a = 0$. In the limit $B \to 0$, (a_c, R_c) and $R(0)$ are

calculated from Eqs. (17) and (18). We note that, in Tables 1 and 2 relative to $s = 1$ and $s = 1/2$ respectively, the values of R_c and $R(0)$ are equal and both expressed by $4\pi^2$. On the contrary, for $s = 1/4$ (Table 3), the values of R_c and $R(0)$ are different as expected from Eq. (18) and displayed in Fig. 2. In fact, for $s = 1/4$, only the mode $(n = 1, m = 1)$ may yield the absolute minimum of $R(a)$, *i.e.* $4\pi^2$, and this is for $a = a_c = \pi$. We mention that, in Tables 1–3, the values of $R(0)$ for $B \to \infty$ are calculated analytically from Eq. (37).

In Section 4.1, we noted that, in the limit $B \to 0$, the m–modes may be associated with either even or odd eigenfunctions $\widetilde{\theta}(x)$. In fact, also for $B > 0$, each branch of neutral stability is associated with a symmetry of the temperature disturbance $\theta(x, y, z)$ with respect to the vertical midplane $x = 0$. With respect to the symmetry of the disturbances, a special interest exists for the critical conditions, *i.e.* at the onset of convection. Figure 11 displays the plots of the isotherms $\theta = constant$ and those of the eigenfunctions $\widetilde{\theta}(x)$ at critical conditions, (a_c, R_c), for $B = 1$ and the three aspect ratios $s = 1, 1/2, 1/4$. It is evident from Fig. 11 that the selected modes of convection at the onset are symmetric with respect to the midplane $y = 0$, *i.e.* the eigenfunctions $\widetilde{\theta}(x)$ at critical conditions are even functions of x.

7.5 Threshold length for the onset of three–dimensional convection

So far, we assumed an infinite longitudinal length of the channel in the z–direction. This implies a continuous spectrum of the wave number a. We may now relax this assumption and assume that, at $z = 0$ and at $z = d$, there exist impermeable and adiabatic boundaries. Here $d = D/H$, where D is the dimensional length of the channel. In this case, the rectangular channel becomes the parallelepiped defined by the dimensionless region $[-s, s] \times [0, 1] \times [0, d]$. The immediate consequence is that the wave number has now a discrete spectrum. From Eq. (13), we infer that the sequence of allowed wave numbers is:

$$a = 0, \frac{\pi}{d}, \frac{2\pi}{d}, \frac{3\pi}{d}, \ \ldots \ . \tag{41}$$

In the previous sections, we pointed out that the absolute minimum of the neutral stability curves $R(a)$ is, in general, for nonvanishing wave numbers. On the basis of the behaviour illustrated in Figs. 3–8, we may affirm that for every assigned transverse aspect ratio s and Biot number B, if a exceeds a sufficiently large threshold value a_{th}, the value of $R(a)$ at neutral stability is greater than $R(0)$. The conclusion is that, if the longitudinal aspect

ratio d is smaller than a threshold value d_{th}, so that the first nonvanishing wave number $a = \pi/d$ is greater than a_{th}, then the onset of convection takes place with $a = 0$ and $R = R(0)$. Stated differently, if $d < d_{th} = \pi/a_{th}$, the onset of convection takes place with a two–dimensional flow pattern ($a = 0$). Otherwise, the onset of convection is with three–dimensional modes ($a > 0$). The value of d_{th}, or of a_{th}, as a function of s and B is thus a sensible quantity to be determined.

In the special case $B \to 0$, the evaluation of a_{th} and d_{th} can be carried out analytically starting from Eqs. (17) and (18). We first point out that, depending on the value of s, we may have either $R(0) = R_c$ or $R(0) > R_c$. In particular, we have $R(0) = R_c$ if s is an integer or a half–integer. Otherwise, we have $R(0) > R_c$. This conclusion can be inferred from Eq. (18). As a consequence, a_{th} and d_{th} can be consistently defined in the limit $B \to 0$ only if s is neither an integer nor a half–integer, so that we proceed under this implicit assumption. We mention that the least neutral stability value of $R(0)$ is for the mode $m = m_0$, where m_0 depends on s and can be evaluated as

$$m_0 = \left\lceil \frac{1 + \sqrt{1 + 16 s^2}}{2} \right\rceil , \tag{42}$$

where $\lceil \cdot \rceil$ denotes the ceiling function, *i.e.* the function giving the smallest integer greater or equal to its argument. The proof of this result, reported also by Sutton [11], is a straightforward consequence of Eq. (17). Figure 2 reveals that the solution of $R(a_{th}) = R(0)$ must be sought in the branch with $m = 1$. Thus, one may conclude from Eqs. (17) and (42) that

$$a_{th} = \max \left(\frac{2\pi s}{m_0 - 1}; \ \frac{(m_0 - 1)\,\pi}{2s} \right) , \qquad d_{th} = \min \left(\frac{m_0 - 1}{2s}; \ \frac{2s}{m_0 - 1} \right) . \tag{43}$$

The trend of d_{th} versus s, shown in Fig. 12, displays cusps for the integer or half–integer values of s, where d_{th} is ill–defined, as well as for

$$s = \frac{1}{2}\sqrt{j(j-1)}, \quad j = 2, 3, 4, \ \ldots \ . \tag{44}$$

Figure 12 displays also the plot of $R(0)$ versus s for $B \to 0$. Cusps are present in this plot for the values of s given by Eq. (44), while local minima, $R(0) = 4\pi^2$, are present for the integer or half–integer values of s. We mention that the values of s defined by Eq. (44) describe the transition between different m–modes as the most unstable when $a = 0$. For instance, for $s = \sqrt{2}/2$ (with $j = 2$) we have the transition from the mode $m = 2$ to the mode $m = 3$.

Except for the limiting case $B \to 0$, the evaluation of a_{th} and d_{th} cannot be done analytically, but only numerically. Figure 12 shows the behaviour of $R(0)$ and that of d_{th} versus s for $B = 1$ (dotted line), and for $B \to \infty$ (dashed line). We see that, for $B = 1$, the trends of both $R(0)$ and d_{th} are oscillating as those for the limiting case $B \to 0$. These oscillations are completely damped in the limit $B \to \infty$. In this limit, $R(0)$ is a monotonic decreasing function of s, expressed analytically by Eq. (37), while d_{th} is a monotonic increasing function of s. Values of a_{th} and d_{th} for different aspect ratios s in the case $B \to \infty$ are reported in Table 4. From the information conveyed in Fig. 12 and in Table 4, we may conclude that three–dimensional convection is generally favoured for small values of s (tall rectangular channels), since the condition $d < d_{th}$ can be fulfilled only with short channels. For instance, we see from Table 4 that, in the case of a transverse aspect ratio $s = 1/4$ and $B \to \infty$, the onset of convection is two–dimensional only if the length of the channel is smaller than approximately one–fourth of its height.

8 Conclusions

The conditions for the linear stability of a fluid saturated porous medium confined in a horizontal rectangular channel with impermeable walls and heated from below have been studied. The analysis has been carried out by assuming that the horizontal boundaries are isothermal with unequal temperatures, while the vertical sidewalls are subject to third–kind temperature boundary conditions. These conditions describe a process of convection to an external fluid environment thermally stratified in the vertical direction. The onset of convection is determined by three governing parameters: the Darcy–Rayleigh number R, the Biot number B associated with the sidewall external convection, and the transverse aspect ratio s. The thermoconvective instability takes place when, for given values of B and s, the Darcy–Rayleigh number exceeds its critical value R_c. The study has been based on the three–dimensional normal mode expansion of the disturbances associated with the pressure field and with the temperature field. The disturbance equations were solved both by the Galerkin method of weighted residuals, and by a numerical solution obtained with a combined numerical Runge–Kutta method and shooting method. We obtained the following main results.

- The critical Darcy–Rayleigh number is an increasing function of the Biot number. In other words, by increasing the conductance across the vertical sidewalls, the fluid saturated

porous medium enhances its stability.

- The value of critical Darcy–Rayleigh number R_c is $4\pi^2$ in the limit $B \to 0$. The onset of convection in this limit can be attained, depending on the aspect ratio s, with one or more possible critical values of the wave number. If s is either an integer or a half–integer, $4\pi^2$ coincides also with the lowest R for neutral stability with $a = 0$, denoted by $R(0)$. This feature is lost when B increases above zero: the value of R_c is lower than $R(0)$. In other words, with $B > 0$, the onset of convection takes place through three–dimensional flow patterns.
- The analysis, performed by assuming an infinitely long channel, has been completed by considering the case of a channel with a finite longitudinal length, bounded by impermeable and adiabatic end sections. We proved that, with a sufficiently small longitudinal length, the onset of convection is two–dimensional, while it becomes three–dimensional when the length–to–height aspect ratio d of the channel exceeds a threshold value d_{th}. The value of d_{th} depends both on B and on s. The observed behaviour is that d_{th} is smaller for tall rectangular channels ($s < 1/2$) than for square ($s = 1/2$) or shallow rectangular channels ($s > 1/2$).

References

[1] C. W. Horton, F. T. Rogers, Convection currents in a porous medium, Journal of Applied Physics 16 (1945) 367–370.

[2] E. R. Lapwood, Convection of a fluid in a porous medium, Proceedings of the Cambridge Philosophical Society 44 (1948) 508–521.

[3] D. A. S. Rees, The stability of Darcy–Bénard convection, in: K. Vafai, H. A. Hadim (Eds.), Handbook of Porous Media, CRC Press, New York, 2000, Ch. 12, pp. 521–558.

[4] P. A. Tyvand, Onset of Rayleigh–Bénard convection in porous bodies, in: D. B. Ingham, I. Pop (Eds.), Transport Phenomena in Porous Media II, Pergamon, New York, 2002, Ch. 4, pp. 82–112.

[5] D. A. Nield, A. Bejan, Convection in Porous Media, 3rd Edition, Springer, New York, 2006.

[6] B. Straughan, The Energy Method, Stability, and Nonlinear Convection, 2nd Edition, Applied Mathematical Sciences Series, Springer, New York, 2010.

[7] A. Barletta, Thermal instabilities in a fluid saturated porous medium, in: A. Öchsner, G. E. Murch (Eds.), Heat Transfer in Multi–Phase Materials, Springer, New York, 2011, pp. 381–414.

[8] L. Storesletten, M. Tveitereid, Natural convection in a horizontal porous cylinder, International Journal of Heat and Mass Transfer 34 (1991) 1959–1968.

[9] A. Barletta, L. Storesletten, Onset of convective rolls in a circular porous duct with external heat transfer to a thermally stratified environment, International Journal of Thermal Sciences 50 (2011) 1374–1384.

[10] D. A. S. Rees, P. A. Tyvand, The Helmholtz equation for convection in two–dimensional porous cavities with conducting boundaries, Journal of Engineering Mathematics 49 (2004) 181–193.

[11] F. M. Sutton, Onset of convection in a porous channel with net through flow, Physics of Fluids 13 (1970) 1931–1934.

[12] J. L. Beck, Convection in a box of porous material saturated with fluid, Physics of Fluids 15 (1972) 1377–1383.

[13] T. Nilsen, L. Storesletten, An analytical study on natural convection in isotropic and anisotropic porous channels, ASME Journal of Heat Transfer 112 (1990) 396–401.

[14] E. O. Holzbecher, Modeling Density-Driven Flow in Porous Media: Principles, Numerics, Software, Springer, 1998.

[15] D. A. S. Rees, P. A. Tyvand, Oscillatory convection in a two–dimensional porous box with asymmetric lateral boundary conditions, Physics of Fluids 16 (2004) 3706–3714.

[16] E. O. Holzbecher, On the relevance of oscillatory convection regimes in porous media – review and numerical experiments, Computers & Fluids 30 (2001) 189–209.

[17] H. S. Nygård, P. A. Tyvand, Onset of convection in a porous box with partly conducting and partly penetrative sidewalls, Transport in Porous Media 84 (2010) 55–73.

[18] H. S. Nygård, P. A. Tyvand, Onset of thermal convection in a vertical porous cylinder with a partly conducting and partly penetrative cylinder wall, Transport in Porous Media 86 (2011) 229–241.

[19] F. P. Incropera, T. L. Bergman, A. S. Lavine, D. P. DeWitt, Fundamentals of Heat and Mass Transfer, 7th Edition, John Wiley & Sons, 2011.

[20] B. A. Finlayson, L. E. Scriven, The method of weighted residuals – A review, Applied Mechanics Reviews 19 (1966) 735–748.

[21] B. A. Finlayson, Method of Weighted Residuals and Variational Principles, Academic Press, 1972.

B	a_c	R_c	$R(0)$
0	$\begin{cases} 0 \\ 2.72070\ \left(\pi\sqrt{3/4}\right) \\ 3.14159\ (\pi) \end{cases}$	39.4784 $(4\pi^2)$	39.4784 $(4\pi^2)$
0.0001	3.14160	39.4786	39.4788
0.001	3.14167	39.4804	39.4824
0.01	3.14237	39.4983	39.5183
0.1	3.14743	39.6635	39.8664
0.2	3.14967	39.8219	40.2314
0.5	3.14260	40.1743	41.2036
1	3.11254	40.5085	42.4912
2	3.05698	40.7884	44.2296
5	2.98855	40.9908	46.5506
10	2.95883	41.0582	47.7894
20	2.94303	41.0909	48.5284
50	2.93334	41.1102	49.0109
100	2.93008	41.1165	49.1780
200	2.92845	41.1197	49.2626
500	2.92747	41.1215	49.3138
1000	2.92714	41.1222	49.3309
∞	2.92681	41.1228	49.3480 $(5\pi^2)$

Table 1: Aspect ratio $s = 1$: critical values of a and R, and values of of the lowest R for neutral stability with $a = 0$

B	a_c	R_c	$R(0)$
0	$\begin{cases} 0 \\ 3.14159\ (\pi) \end{cases}$	39.4784 $(4\pi^2)$	39.4784 $(4\pi^2)$
0.0001	3.14161	39.4788	39.4792
0.001	3.14175	39.4824	39.4864
0.01	3.14318	39.5183	39.5583
0.1	3.15688	39.8687	40.2692
0.2	3.17098	40.2404	41.0416
0.5	3.20701	41.2538	43.2519
1	3.25042	42.6568	46.5960
2	3.29733	44.6885	52.1476
5	3.32011	47.7183	62.3696
10	3.29664	49.5008	69.4425
20	3.26374	50.6082	73.9969
50	3.23289	51.3407	76.9541
100	3.22035	51.5948	77.9554
200	3.21363	51.7235	78.4564
500	3.20944	51.8011	78.7568
1000	3.20802	51.8271	78.8568
∞	3.20659	51.8531	78.9568 $(8\pi^2)$

Table 2: Aspect ratio $s = 1/2$: critical values of a and R, and values of of the lowest R for neutral stability with $a = 0$

B	a_c	R_c	$R(0)$
0	3.14159 (π)	39.4784 ($4\pi^2$)	61.6850 ($25\pi^2/4$)
0.0001	3.14162	39.4792	61.6860
0.001	3.14191	39.4864	61.6950
0.01	3.14477	39.5583	61.7850
0.1	3.17265	40.2673	62.6799
0.2	3.20223	41.0349	63.6645
0.5	3.28320	43.2190	66.5579
1	3.39703	46.5133	71.1849
2	3.56897	52.0681	79.7506
5	3.85307	63.4210	100.755
10	4.03602	73.5194	124.527
20	4.13959	82.2253	150.012
50	4.18388	89.4962	175.093
100	4.18982	92.3489	185.689
200	4.19021	93.8607	191.411
500	4.18947	94.7952	194.970
1000	4.18904	95.1112	196.176
∞	4.18853	95.4295	197.392 ($20\pi^2$)

Table 3: Aspect ratio $s = 1/4$: critical values of a and R, and values of of the lowest R for neutral stability with $a = 0$

s	a_{th}	d_{th}
1/16	43.7362	0.0718305
3/40	36.5216	0.0860201
7/80	31.3798	0.100115
1/10	27.5333	0.114102
1/8	22.1715	0.141695
3/20	18.6223	0.168701
1/5	14.2400	0.220618
1/4	11.6644	0.269331
3/10	9.98781	0.314543
2/5	7.96927	0.394213
1/2	6.82349	0.460409
3/5	6.09964	0.515046
7/10	5.60739	0.560260
4/5	5.25381	0.597965
9/10	4.98881	0.629728
1	4.78336	0.656776
3/2	4.20165	0.747705
2	3.92826	0.799742
5/2	3.76846	0.833655
3	3.66320	0.857609

Table 4: Limit $B \to \infty$: values of a_{th} and d_{th} for different aspect ratios s

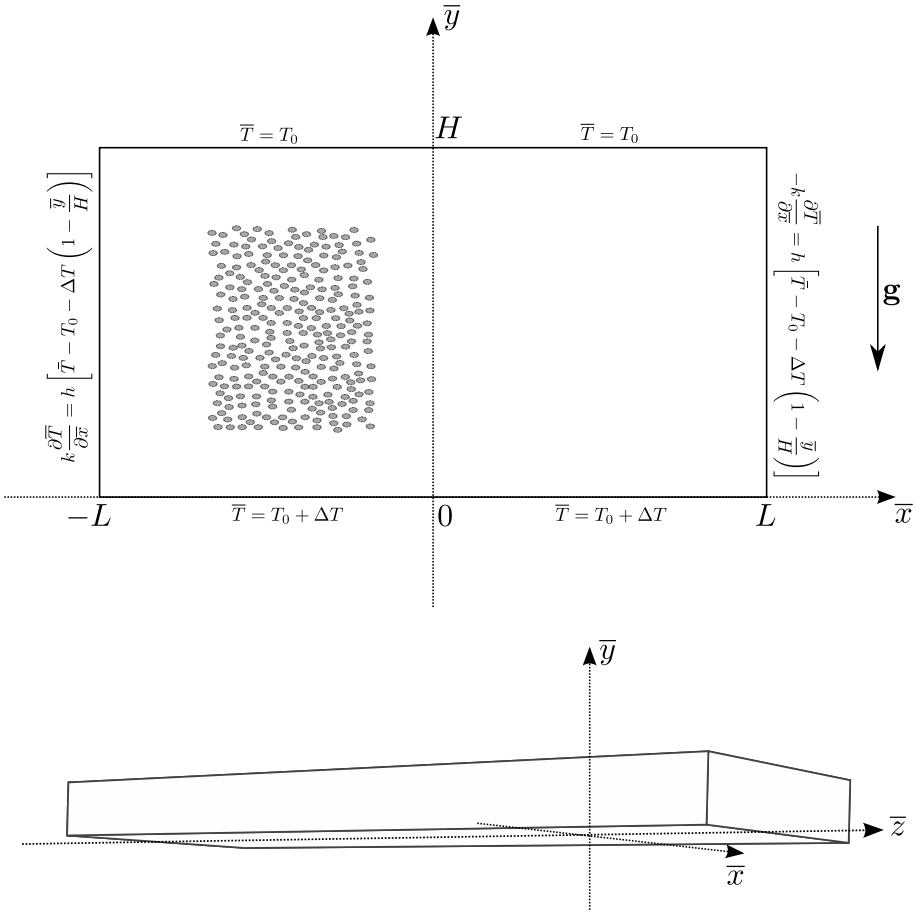

Figure 1: A sketch of the porous channel and of the thermal boundary conditions

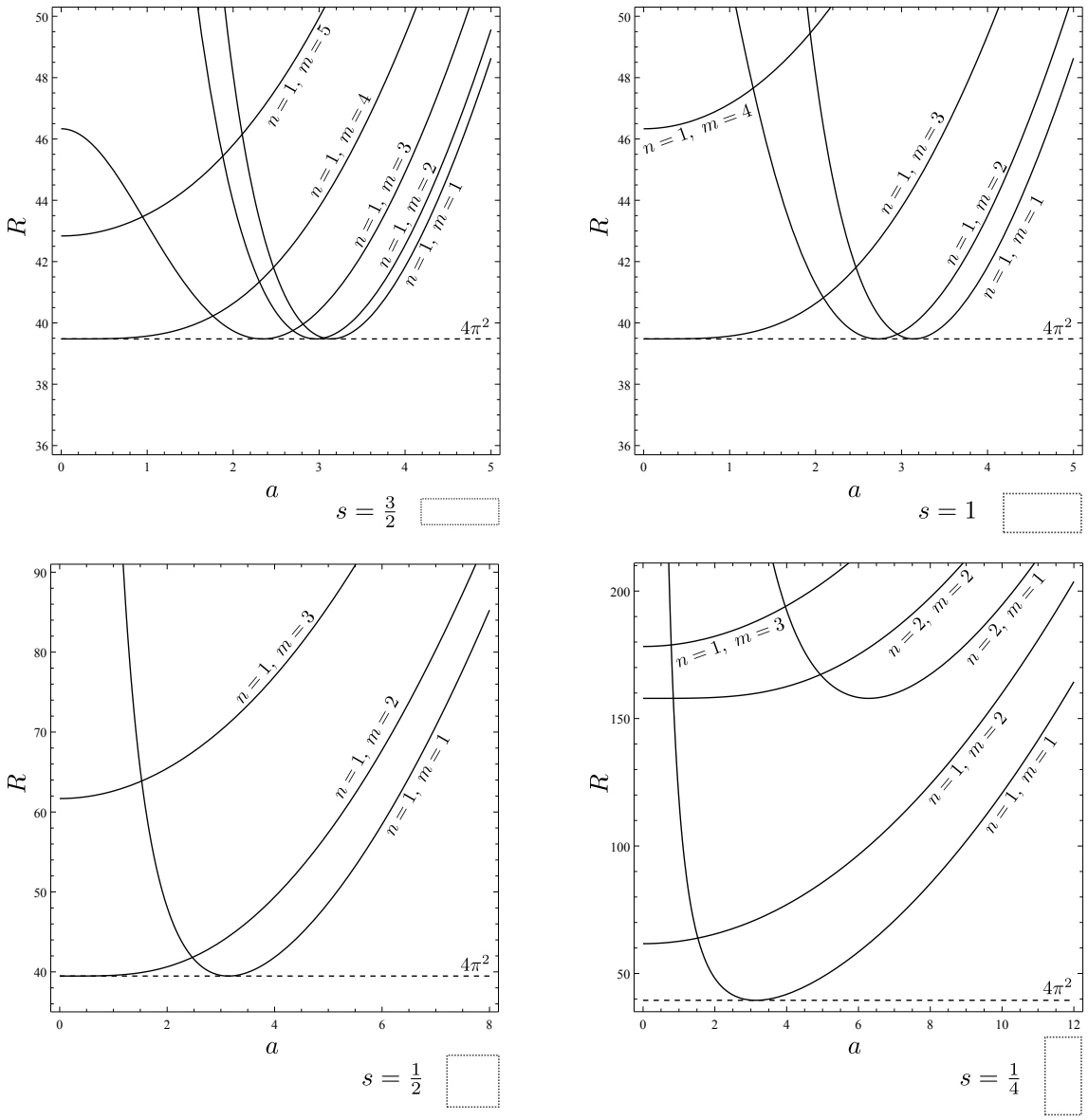

Figure 2: Limit $B \to 0$: neutral stability curves for different aspect ratios and different m–modes; the dashed line is for $R_c = 4\pi^2$

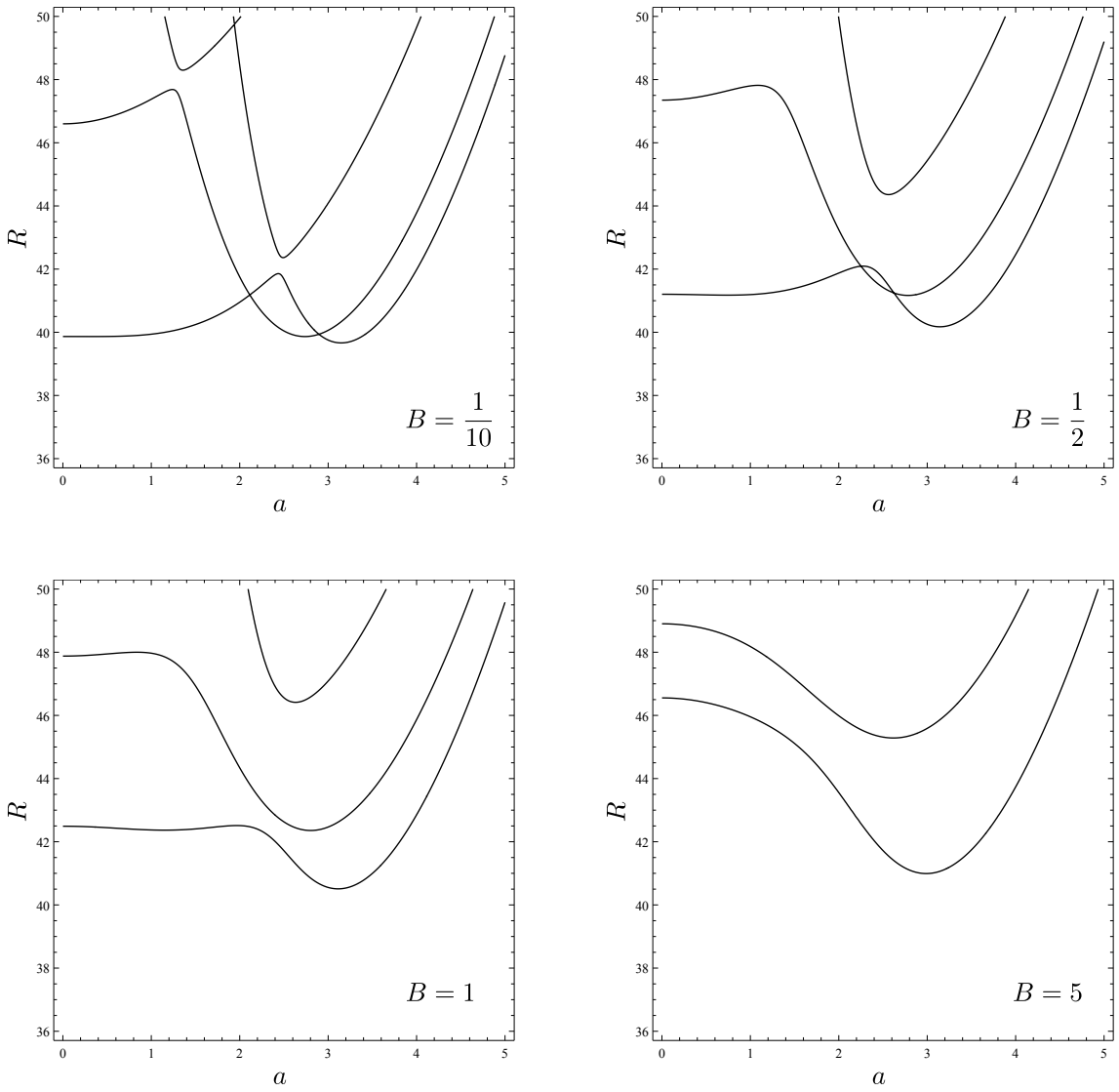

Figure 3: Aspect ratio $s = 1$: neutral stability curves for $B = 1/10, 1/2, 1, 5$; only the curves for the mode $n = 1$ appear in the plotting area

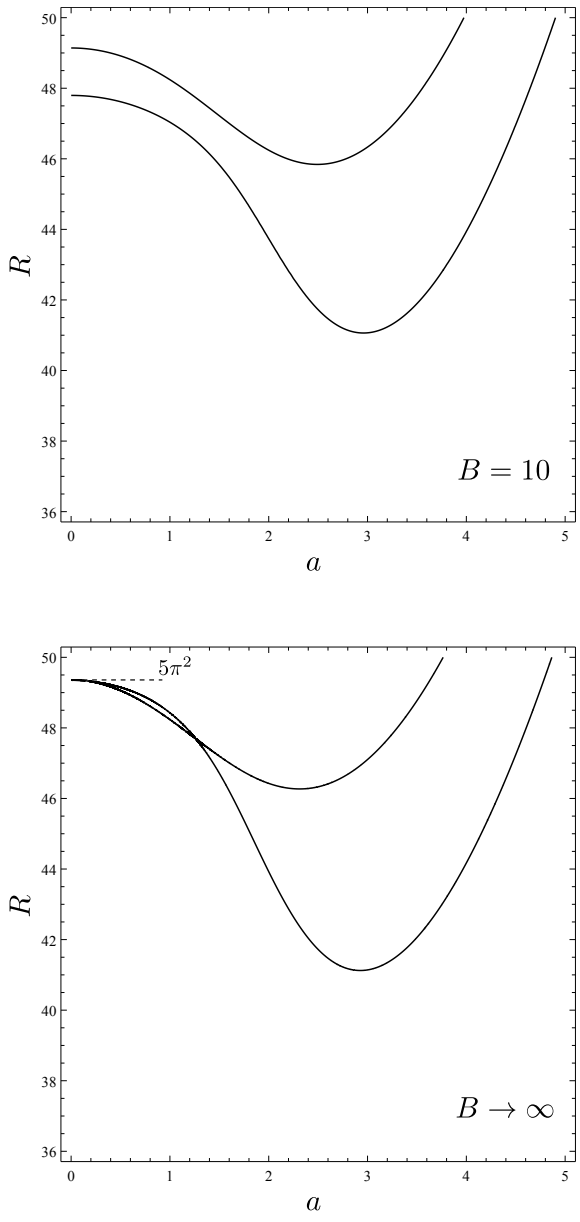

Figure 4: Aspect ratio $s = 1$: neutral stability curves for $B = 10, \infty$; only the curves for the mode $n = 1$ appear in the plotting area

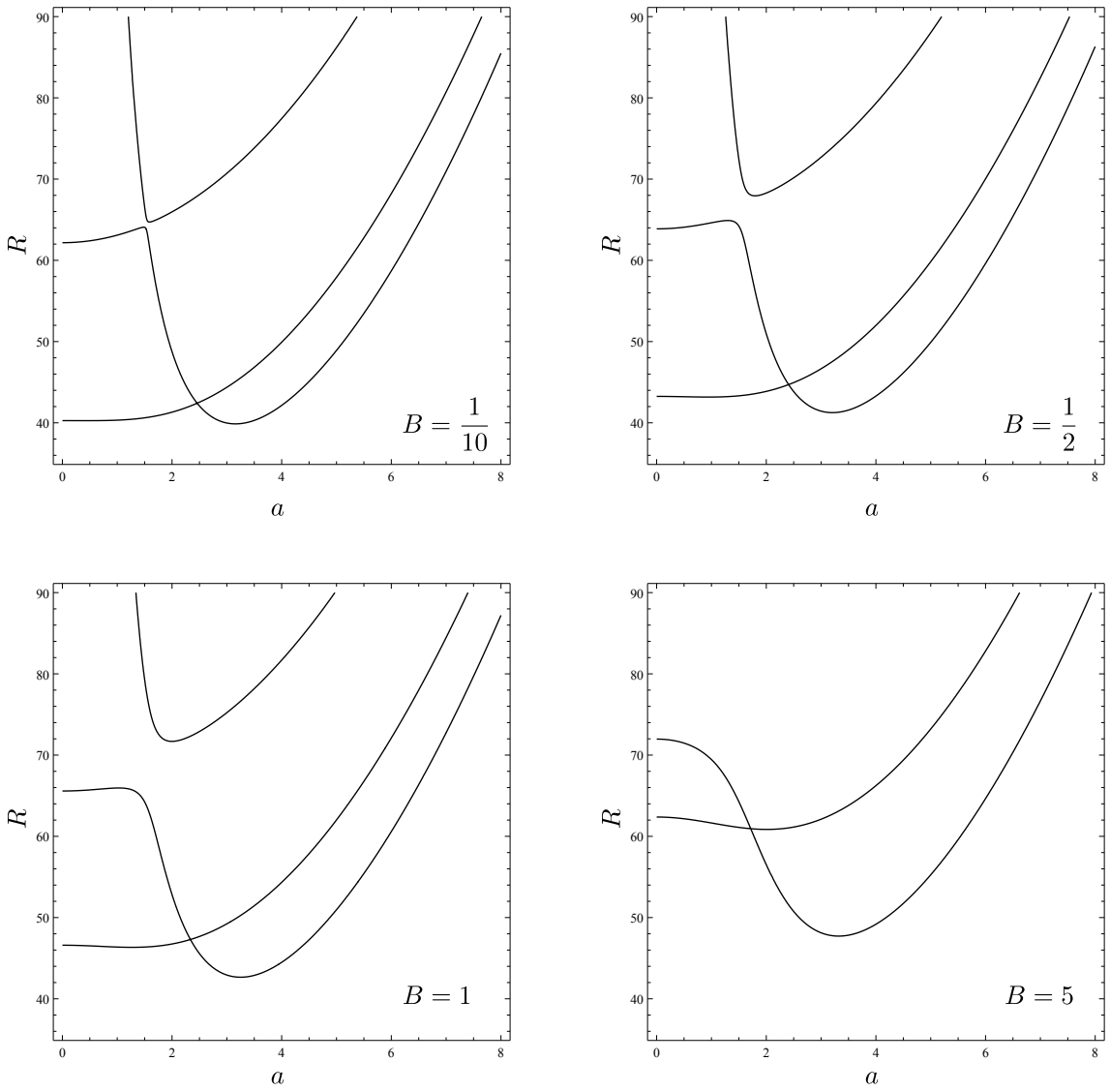

Figure 5: Aspect ratio $s = 1/2$: neutral stability curves for $B = 1/10, 1/2, 1, 5$; only the curves for the mode $n = 1$ appear in the plotting area

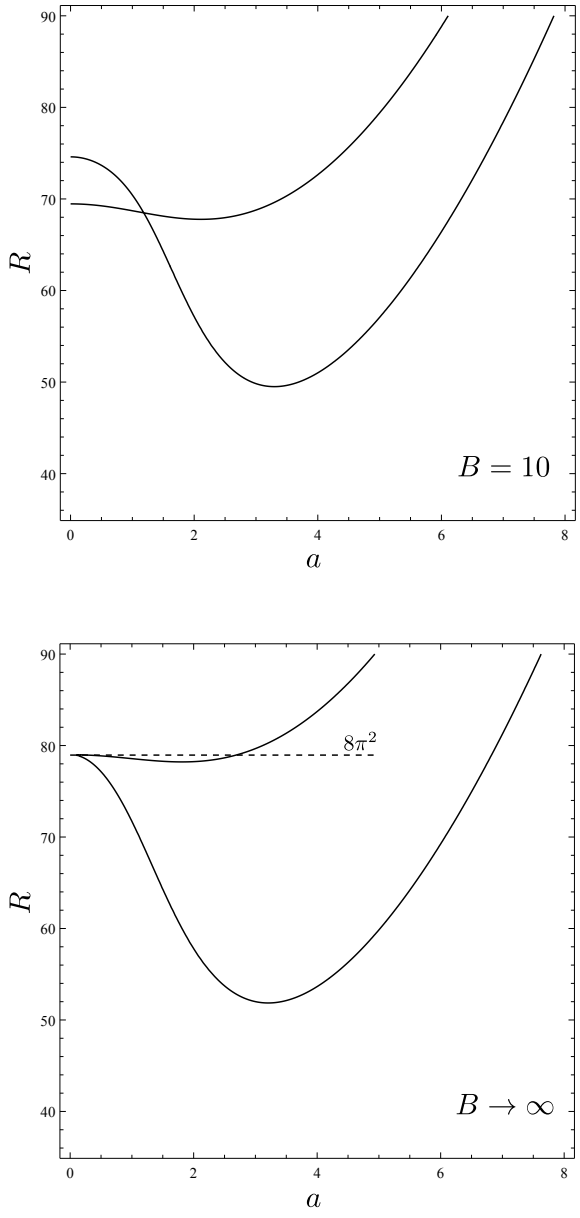

Figure 6: Aspect ratio $s = 1/2$: neutral stability curves for $B = 10, \infty$; only the curves for the mode $n = 1$ appear in the plotting area

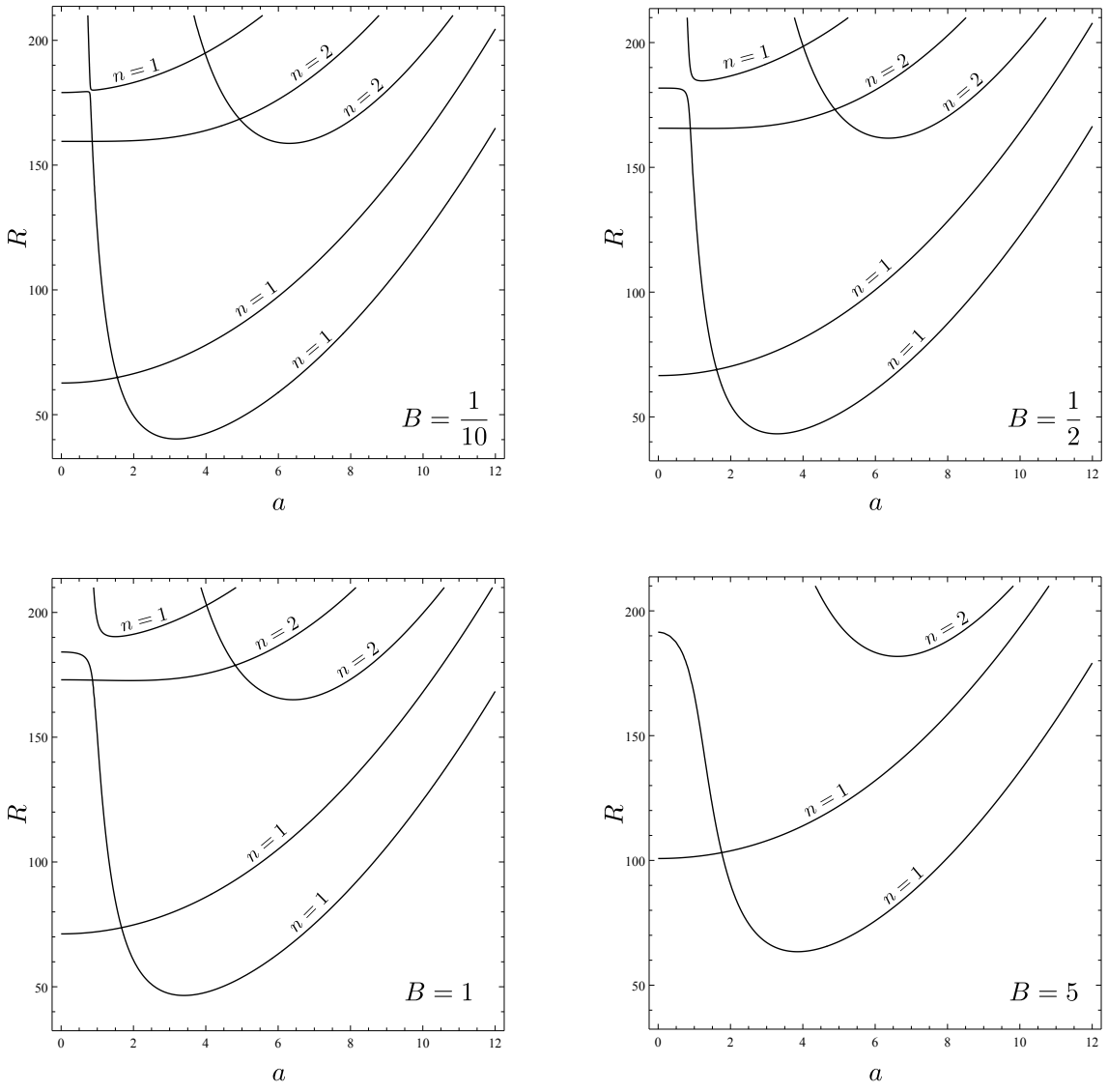

Figure 7: Aspect ratio $s = 1/4$: neutral stability curves for $B = 1/10, 1/2, 1, 5$

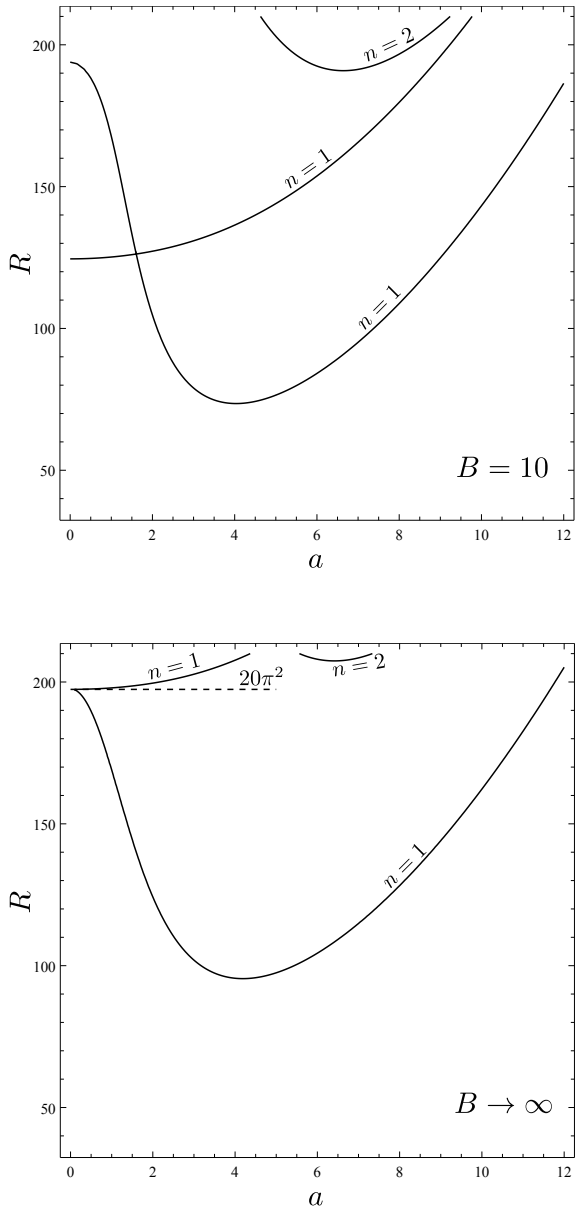

Figure 8: Aspect ratio $s = 1/4$: neutral stability curves for $B = 10, \infty$

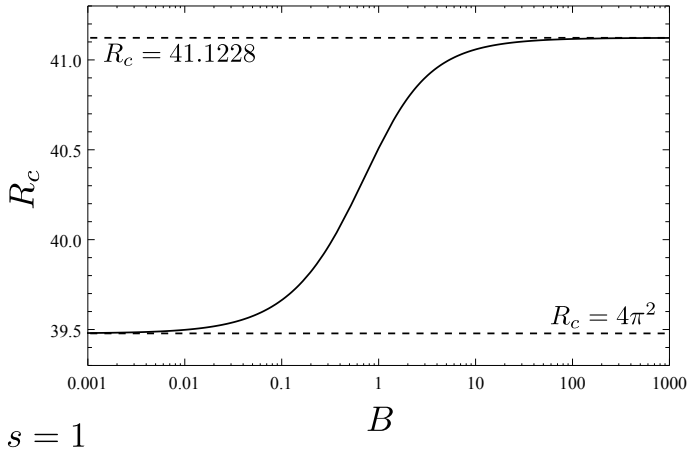

$s = 1$

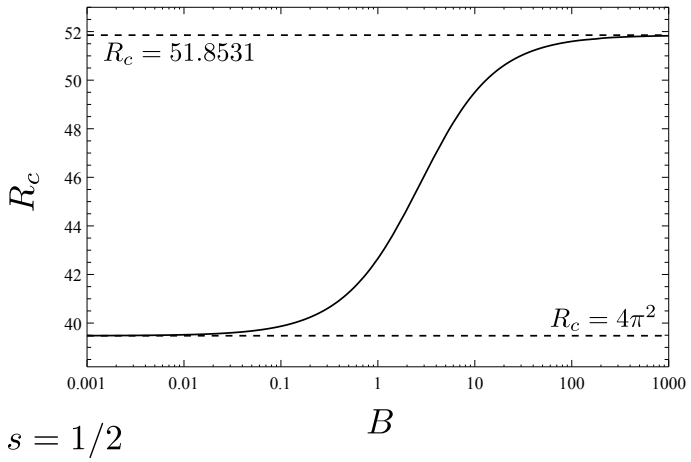

$s = 1/2$

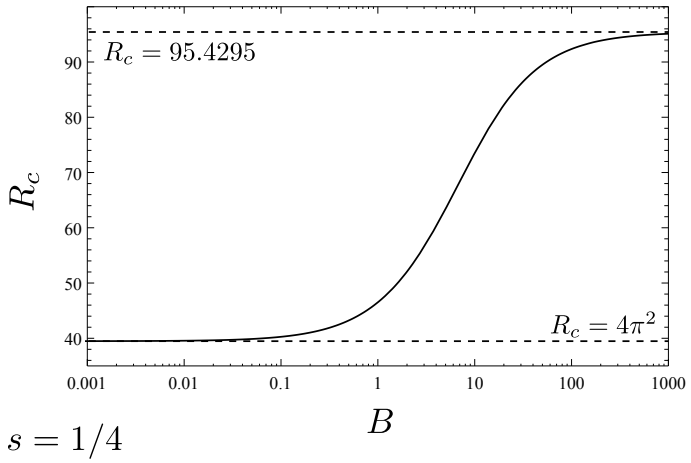

$s = 1/4$

Figure 9: Plots of R_c versus B for the aspect ratios $s = 1, 1/2, 1/4$

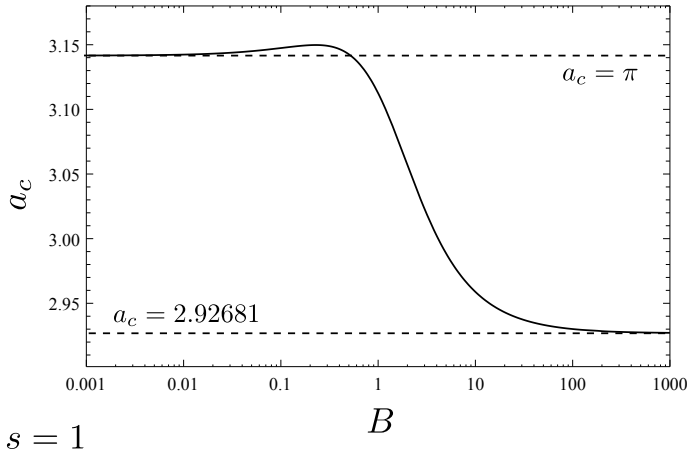

$s = 1$

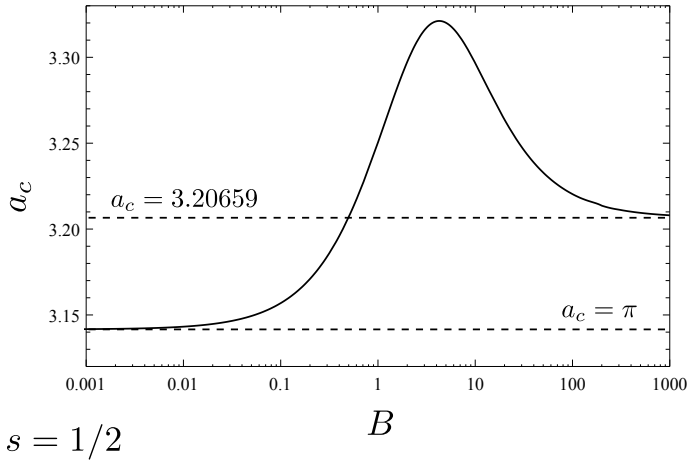

$s = 1/2$

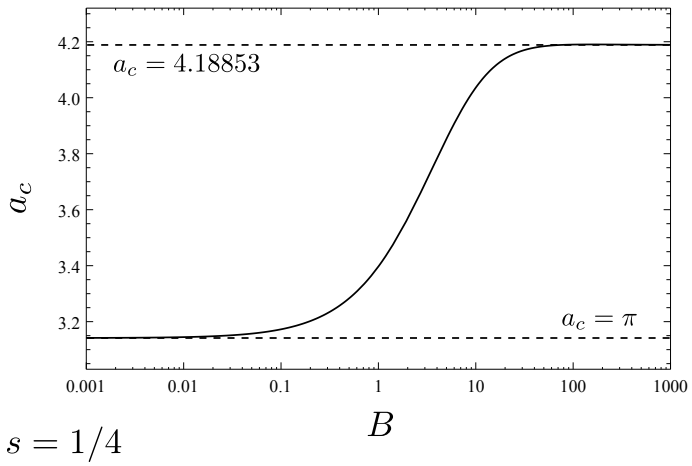

$s = 1/4$

Figure 10: Plots of a_c versus B for the aspect ratios $s = 1, 1/2, 1/4$

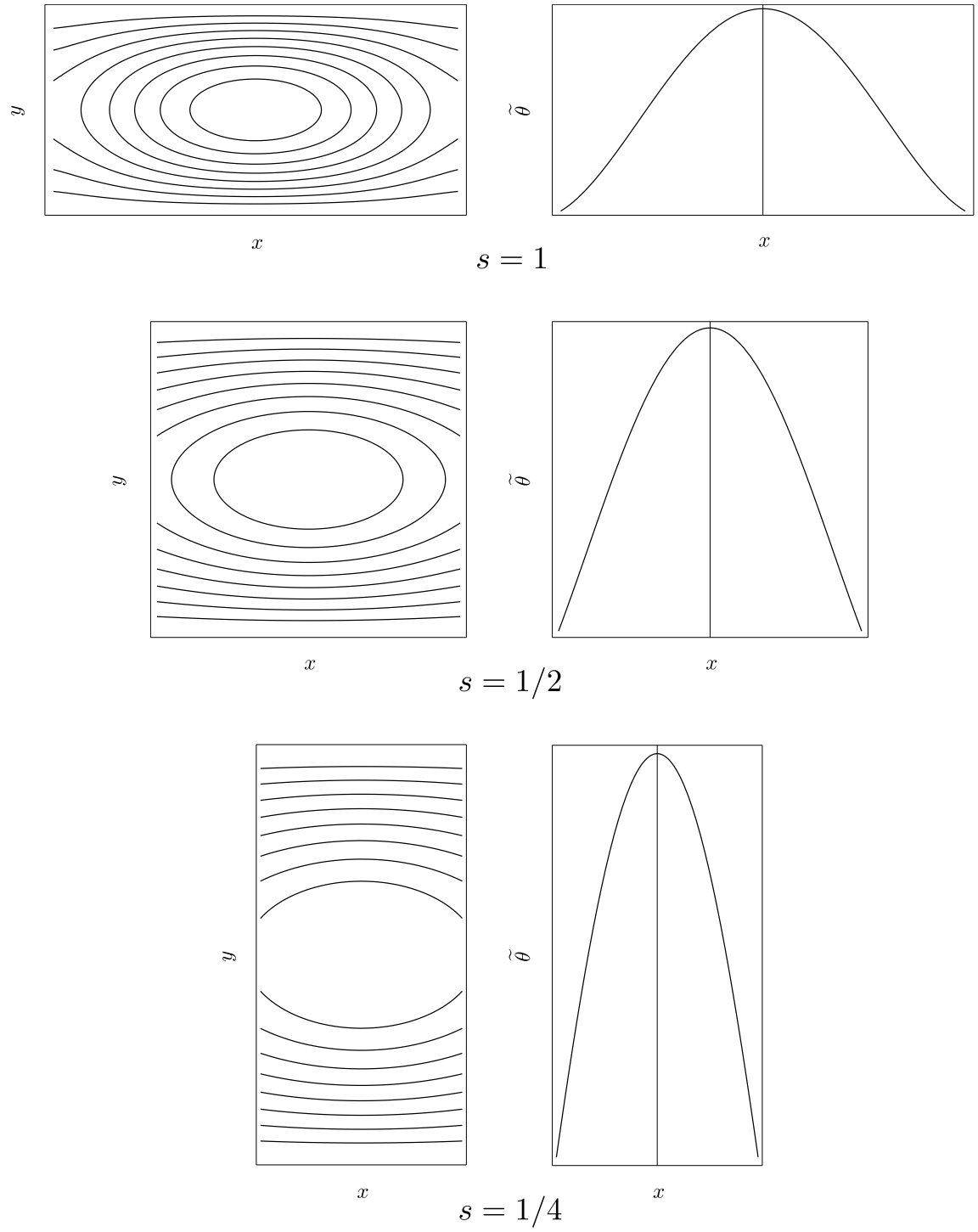

Figure 11: Critical conditions at the onset of convection for $B = 1$: plots of the isotherms $\theta(x, y, z) = constant$ for $z = 0$ (on the left) and plots of $\widetilde{\theta}(x)$ (on the right) for the aspect ratios $s = 1, 1/2, 1/4$

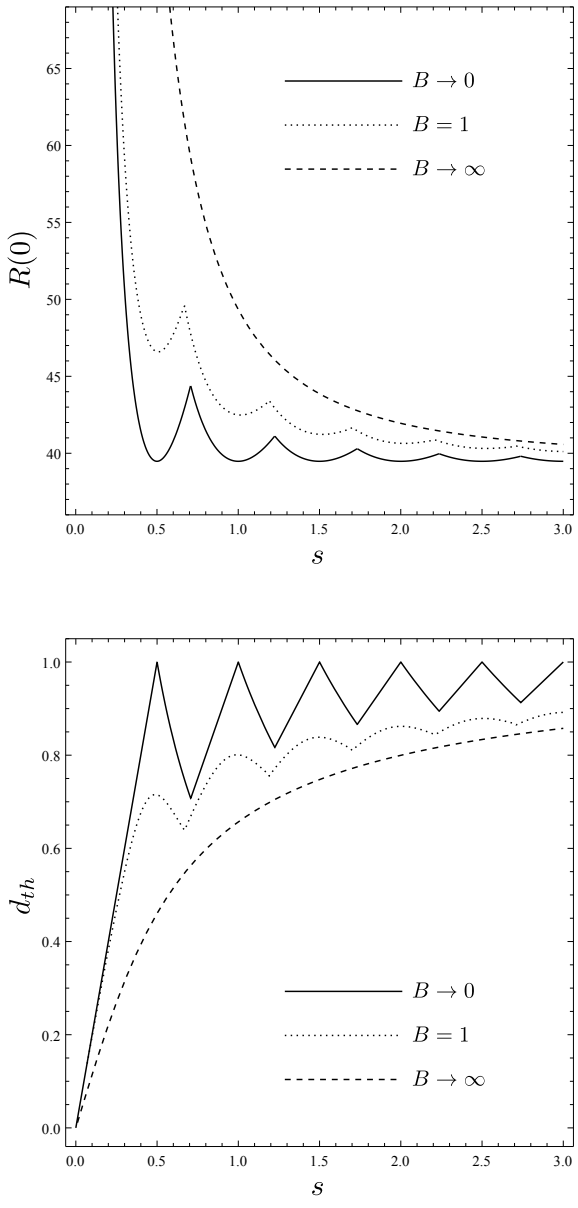

Figure 12: Plots of $R(0)$ versus s, and plots of the threshold longitudinal aspect ratio, d_{th}, versus s